AMERICAN SOCIETY FOR MICROBIOLOGY | Applied and Environmental Microbiology®

PHYSIOLOGY

Quorum Sensing Regulators AphA and OpaR Control Expression of the Operon Responsible for Biosynthesis of the Compatible Solute Ectoine

Gwendolyn J. Gregory,[a] Daniel P. Morreale,[a] Megan R. Carpenter,[a] Sai S. Kalburge,[a] E. Fidelma Boyd[a]

[a]Department of Biological Sciences, University of Delaware, Newark, Delaware, USA

ABSTRACT To maintain the turgor pressure of the cell under high osmolarity, bacteria accumulate small organic compounds called compatible solutes, either through uptake or biosynthesis. *Vibrio parahaemolyticus*, a marine halophile and an important human and shellfish pathogen, has to adapt to abiotic stresses such as changing salinity. *Vibrio parahaemolyticus* contains multiple compatible solute biosynthesis and transporter systems, including the *ectABC-asp_ect* operon required for *de novo* ectoine biosynthesis. Ectoine biosynthesis genes are present in many halotolerant bacteria; however, little is known about the mechanism of regulation. We investigated the role of the quorum sensing master regulators OpaR and AphA in *ect* gene regulation. In an *opaR* deletion mutant, transcriptional reporter assays demonstrated that *ect* expression was induced. In an electrophoretic mobility shift assay, we showed that purified OpaR bound to the *ect* regulatory region indicating direct regulation by OpaR. In an *aphA* deletion mutant, expression of the *ect* genes was repressed, and purified AphA bound upstream of the *ect* genes. These data indicate that AphA is a direct positive regulator. CosR, a Mar-type regulator known to repress *ect* expression in *V. cholerae*, was found to repress *ect* expression in *V. parahaemolyticus*. In addition, we identified a feed-forward loop in which OpaR is a direct activator of *cosR*, while AphA is an indirect activator of *cosR*. Regulation of the ectoine biosynthesis pathway via this feed-forward loop allows for precise control of ectoine biosynthesis genes throughout the growth cycle to maximize fitness.

IMPORTANCE Accumulation of compatible solutes within the cell allows bacteria to maintain intracellular turgor pressure and prevent water efflux. *De novo* ectoine production is widespread among bacteria, and the *ect* operon encoding the biosynthetic enzymes is induced by increased salinity. Here, we demonstrate that the quorum sensing regulators AphA and OpaR integrate with the osmotic stress response pathway to control transcription of ectoine biosynthesis genes in *V. parahaemolyticus*. We uncovered a feed-forward loop wherein quorum sensing regulators also control transcription of *cosR*, which encodes a negative regulator of the *ect* operon. Moreover, our data suggest that this mechanism may be widespread in *Vibrio* species.

KEYWORDS CosR, compatible solute, ectoine, quorum sensing, regulation

In response to osmotic stress, bacteria have developed a strategy that involves accumulation of compatible solutes through uptake from the environment or biosynthesis from available precursors to maintain the turgor pressure of the cell. Compatible solutes are small organic compounds which bacteria can accumulate in the cell without disrupting cellular processes to counteract increased external osmolarity (1–3). As a marine organism, *Vibrio parahaemolyticus*, a halophile, encounters fluctuations in osmolarity to which it must rapidly respond to prevent cell lysis. *Vibrio parahaemolyti-*

Citation Gregory GJ, Morreale DP, Carpenter MR, Kalburge SS, Boyd EF. 2019. Quorum sensing regulators AphA and OpaR control expression of the operon responsible for biosynthesis of the compatible solute ectoine. Appl Environ Microbiol 85:e01543-19. https://doi.org/10.1128/AEM.01543-19.

Editor Eric V. Stabb, University of Illinois at Chicago

Copyright © 2019 American Society for Microbiology. All Rights Reserved.

Address correspondence to E. Fidelma Boyd, fboyd@udel.edu.

Received 8 July 2019
Accepted 9 September 2019
Accepted manuscript posted online 13 September 2019
Published 30 October 2019

Downloaded from http://aem.asm.org/ on May 1, 2020 by guest

cus has biosynthesis pathways for the compatible solutes ectoine (*ectABC-asp_ect*) and glycine betaine (*betIBA*) and at least six transporters for compatible solute uptake (4–6).

Aspartic acid is the precursor for ectoine, which can be biosynthesized *de novo*. Aspartic acid is converted to ectoine by EctA, EctB, and EctC encoded by the operon *ectABC*, which is evolutionarily conserved in Gram-positive and Gram-negative bacteria (7–9). Several species that produce ectoine also encode a dedicated aspartokinase (Ask) specific to the ectoine biosynthesis pathway, which is clustered with the *ectABC* genes (10–13). All *Vibrio* species contain an aspartokinase (Asp_Ect) in the same operon as the *ectABC* genes (4). Ectoine production was shown to be essential for growth of *V. parahaemolyticus* in minimal medium supplemented with 6% NaCl when no other compatible solutes or precursors are available (5). Ectoine is a bona fide compatible solute and cannot be used as a carbon source by *V. parahaemolyticus*. Ectoine biosynthesis genes in *V. parahaemolyticus* are induced by NaCl upshock during exponential phase and repressed in stationary phase; however, the mechanism of transcriptional control remains unknown (5). EctR1 and CosR were identified as local regulators of ectoine biosynthesis in *Methylmicrobium alcaliphilum* and *V. cholerae*, respectively (14, 15). EctR1, a member of the multiple antibiotic resistance (MarR)-type regulators, in the halotolerant methanotroph *M. alcaliphilum*, repressed expression of the *ectABC-asp_ect* operon in response to salinity (14). In *V. cholerae*, CosR shared 51% sequence identity to EctR1 and was also identified as a repressor of ectoine biosynthesis genes under low-salinity conditions (15).

Quorum sensing is a form of bacterial communication used to coordinate behaviors in response to changing cell density. The quorum sensing circuitry has been studied extensively in *V. harveyi*, and a similar system with a LuxR homologue, OpaR, has been demonstrated in *V. parahaemolyticus* (16–22). Quorum sensing involves the synthesis of autoinducers (AIs), which bind to receptors, triggering a phosphorelay pathway that activates LuxO, the master response regulator. In *V. harveyi*, at a low cell density, the concentration of AIs in the environment is low, and therefore the receptors act as kinases, leading to the phosphorylation of LuxO (23, 24). LuxO is an activator of the sigma factor RpoN, which activates the transcription of five homologous small regulatory RNAs (sRNAs) named quorum regulatory RNAs (Qrr1 to Qrr5) (25, 26). Qrr sRNAs hybridize with *aphA* or *opaR* transcripts to promote their translation or degradation, respectively (18, 27–29). AphA is therefore upregulated at low cell density and regulates hundreds of genes (30). At a high cell density, LuxO is inactive, no Qrr sRNAs are transcribed, and LuxR, the high-cell-density master regulator, is produced to regulate hundreds of genes. In addition, LuxR and AphA are autoregulators and negatively regulate each other (18, 23, 27, 28, 30, 31). Previously, it was shown that LuxR in *V. harveyi* positively regulates glycine betaine biosynthesis genes (32). In *V. parahaemolyticus*, it was demonstrated that the ectoine biosynthesis genes were repressed in a *luxO* mutant (where OpaR levels are high) compared to the wild type (WT) (22).

In this study, we determined the role of global and local regulators in the control of expression of the ectoine biosynthesis *ectABC-asp_ect* operon. We examined expression of ectoine biosynthesis genes across the growth cycle in *V. parahaemolyticus* RIMD2210633 and determined expression in quorum sensing deletion Δ*luxO*, Δ*aphA*, and Δ*opaR* mutants and in Δ*opaR* Δ*aphA* and Δ*luxO* Δ*opaR* double mutants using plasmid-based transcriptional fusion reporter assays. We demonstrated a role for AphA and OpaR in ectoine gene expression and used DNA binding assays to determine whether regulation was direct or indirect. We examined the *V. parahaemolyticus* CosR (VP1906) regulator and uncovered a feed-forward loop involving both AphA and OpaR. This study demonstrates that the quorum sensing regulators AphA and OpaR, as well as CosR, play a role in transcriptional regulation of the *ectABC-asp_ect* operon.

RESULTS

Expression of *ectABC-asp_ect* and quorum sensing regulator genes throughout the growth cycle. Previously, we showed that in a quorum sensing Δ*luxO* deletion mutant the *ect* genes were repressed compared to the wild type (22). To determine the

Downloaded from http://aem.asm.org/ on May 1, 2020 by guest

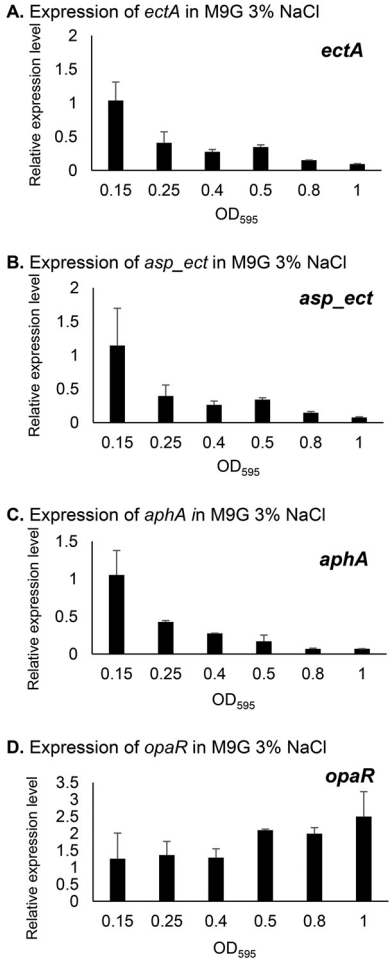

FIG 1 Expression analysis of *ectA*, *asp_ect*, *aphA*, and *opaR* across the growth curve by quantitative real-time PCR (qPCR). RNA was isolated from WT at an OD_{595} of 0.15, 0.25, 0.4, 0.5, 0.8, or 1.0 after growth in M9G3%. qPCR was performed using primer sets for *ectA* (A), *asp_ect* (B), *aphA* (C), and *opaR* (D), and 16S was used for normalization. The expression levels shown are relative to the levels for each gene at an OD_{595} of 0.15. Means and standard errors for at least two biological replicates are shown.

expression pattern of the ectoine biosynthesis operon *ectABC-asp_ect* in *V. parahaemolyticus* across the growth curve, we examined expression levels in M9G3% (see Materials and Methods for descriptions of media) at optical densities at 595 nm (OD_{595}s) of 0.15, 0.25, 0.4, 0.5, 0.8, and 1.0. We found that the ectoine biosynthesis genes *ectA* and *asp_ect* are most highly expressed in early-exponential-phase cells (OD_{595} of 0.15) and that the expression levels decrease with increasing OD (Fig. 1A and B). Next, we examined the expression levels of *aphA* and/or *opaR* under the same conditions and at the same growth time points to determine whether there was a correlation with ectoine gene expression. We found that *aphA* is most highly expressed during early exponential phase and that *opaR* is most highly expressed in the late exponential and stationary phases (Fig. 1C and D). These data suggest that the *ect* genes could be under the control of the quorum sensing master regulators AphA and OpaR.

Ectoine biosynthesis genes are differentially regulated in quorum sensing mutants. We investigated the contribution of AphA and OpaR to ectoine biosynthesis gene expression by measuring the transcriptional activity of the *ect* regulatory region using a transcriptional fusion green fluorescent protein (GFP) reporter assay. The P_{ectA}-*gfp* reporter was examined in the WT and in the quorum sensing Δ*luxO*, Δ*aphA*, and Δ*opaR* deletion mutants. Strains were grown overnight in M9G3%, and the relative

Downloaded from http://aem.asm.org/ on May 1, 2020 by guest

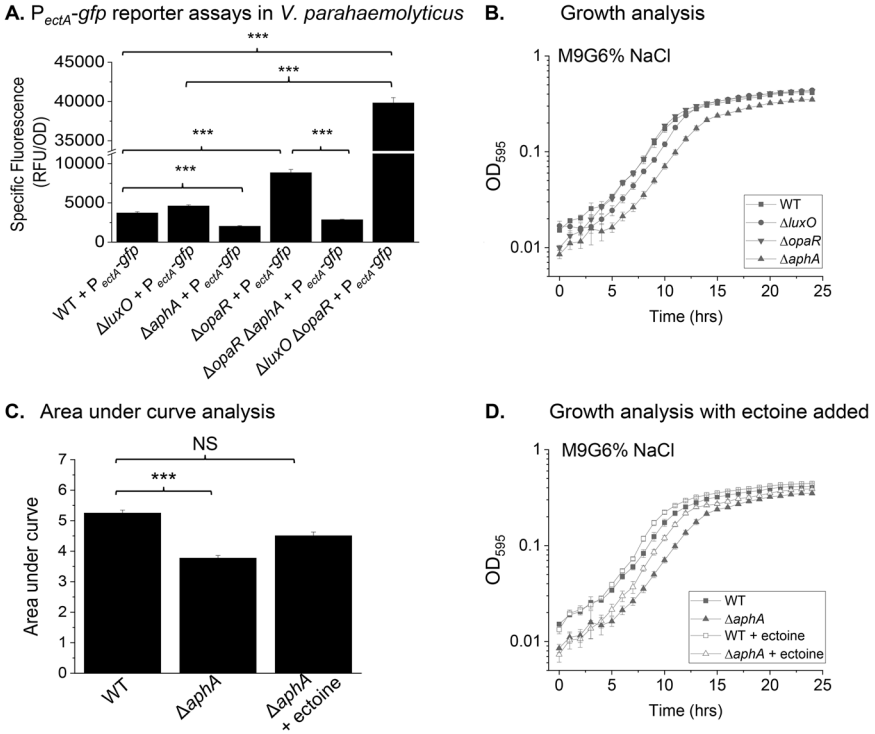

FIG 2 (A) Expression of a P_{ectA}-*gfp* transcriptional fusion in wild-type (WT) *V. parahaemolyticus* and in Δ*luxO*, Δ*aphA*, Δ*opaR*, Δ*opaR* Δ*aphA*, and Δ*luxO* Δ*opaR* mutants. Cultures were grown overnight in M9G3%, and the relative fluorescence intensity (RFU) was measured. The specific fluorescence was calculated by dividing the RFU by the OD. Means and standard deviations of at least two biological replicates are shown. Statistics were calculated using a one-way ANOVA with a Tukey-Kramer *post hoc* test (**, $P < 0.001$). (B) Growth analysis of WT, Δ*luxO*, Δ*aphA*, and Δ*opaR* mutant strains was conducted in M9G6%. (C) The area under the curve of WT and Δ*aphA* strains after 24 h of growth in M9G6% in the growth analysis was calculated using Origin 2018 and compared to area under the curve of the Δ*aphA* mutant grown in M9G6% with the addition of 100 μM ectoine. Means and standard errors were plotted. Statistics were calculated using a one-way ANOVA with a Tukey-Kramer *post hoc* test (***, $P < 0.001$; NS, not significant). (D) Growth analysis of WT and Δ*aphA* strains in M9G6% or M9G6% supplemented with 100 μM ectoine. Means and standard errors were plotted, with the results for two biological replicates shown.

fluorescence intensity was then normalized to OD_{595}. In the Δ*luxO* mutant, the overall P_{ectA}-*gfp* activity was unchanged compared to the WT, whereas the P_{ectA}-*gfp* expression levels in the Δ*aphA* mutant were significantly downregulated (Fig. 2A). Compared to the WT, P_{ectA}-*gfp* expression levels in the Δ*opaR* mutant were significantly upregulated (Fig. 2A). Since AphA and OpaR are negative regulators of each other, these data could indicate that OpaR is a negative regulator and/or that AphA is a positive regulator of ectoine biosynthesis gene expression. To investigate this further, we determined the overall P_{ectA}-*gfp* expression in both Δ*opaR* Δ*aphA* and Δ*luxO* Δ*opaR* double mutants (Fig. 2A). The P_{ectA}-*gfp* expression level was significantly downregulated (3.10-fold) in the Δ*opaR* Δ*aphA* double mutant compared to the levels in the Δ*opaR* mutant (Fig. 2A); this demonstrates that AphA is a positive regulator. When *opaR* is deleted in the Δ*luxO* mutant background, P_{ectA}-*gfp* activity in this double mutant is increased 10.73-fold compared to WT and 8.64-fold compared to the Δ*luxO* single mutant (Fig. 2A). These data demonstrate that OpaR is a negative regulator of the *ectABC-asp_ect* operon.

The *aphA* mutant has a growth defect under high-salt conditions. To grow in high-salinity media without exogenous compatible solutes, *V. parahaemolyticus* needs to produce ectoine (5). We investigated the growth of each of the quorum sensing mutant strains compared to growth of the WT under high-salt-stress conditions (M9G6%). The Δ*opaR* mutant strain grew similarly to the WT (Fig. 2B), whereas the Δ*aphA* mutant strain had a growth defect in M9G6% (Fig. 2B). The Δ*luxO* mutant also

Downloaded from http://aem.asm.org/ on May 1, 2020 by guest

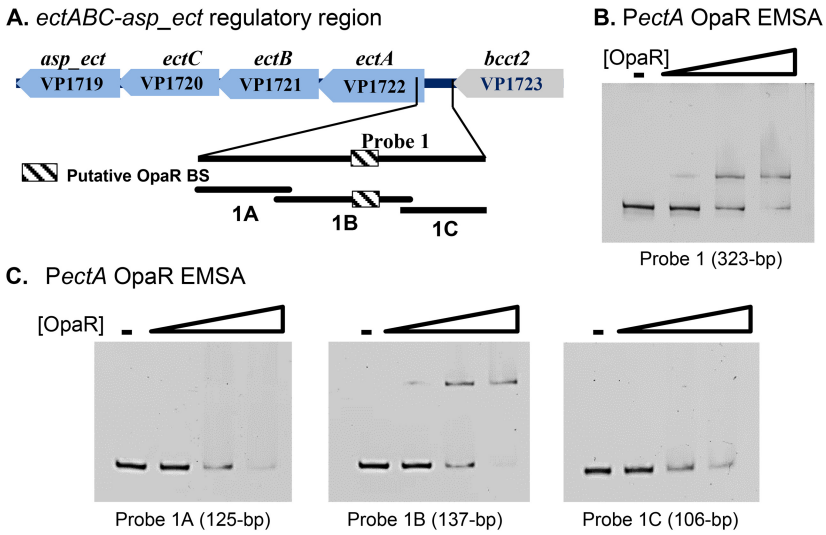

FIG 3 (A) The region upstream of *ectABC-asp_ect* (P*ectA*) is shown with a putative OpaR binding site 166 bp upstream of the translational start. P*ectA* Probe 1, 323 bp in length, comprises the entirety of the *ectABC-asp_ect* regulatory region (positions +33 to −290 relative to the ATG) and contains the putative OpaR binding site. P*ectA* probe 1 was then subdivided into three similarly sized probes, with probe 1B containing the putative OpaR binding site. An EMSA was performed with various concentrations of purified OpaR protein (0 to 0.87 μM) and 30 ng of probe 1 (B) or probes 1A, 1B, and 1C (125, 137, and 106 bp in length, respectively) (C), with DNA/protein ratios of 1:0, 1:1, 1:10, and 1:20.

had a defect, but it was not as pronounced as in the Δ*aphA* mutant. We quantified the growth defect by calculating the area under the curve for both the WT and the Δ*aphA* mutant and found there was a significant difference, indicating a reduced osmotic tolerance in the Δ*aphA* mutant (Fig. 2C). When the Δ*aphA* mutant was supplemented with exogenous ectoine in the growth media, there was no longer a significant difference in growth between the two strains (Fig. 2C and D). This suggests that reduced ectoine production is responsible for the reduced osmotic tolerance of the Δ*aphA* mutant.

OpaR and AphA bind upstream of the ectoine biosynthesis operon. To further demonstrate that AphA and OpaR are regulators of the ectoine biosynthesis genes, we performed bioinformatics analysis to identify putative binding sites for each regulator in the *ect* operon regulatory region. To accomplish this, we utilized a suite of algorithms (MOODS), which uses a known position frequency matrix for each regulatory protein to calculate the probability of binding to a given sequence of DNA (33). We used the previously published OpaR consensus binding sequence (20, 21) and determined that OpaR has a putative binding site 166 to 187 bp upstream of the *ectA* translation start (Fig. 3A). To test whether OpaR binds directly to the regulatory region, electrophoretic mobility shift assays (EMSAs) were performed using purified protein and DNA probes containing the putative binding site. OpaR bound to P*ectA* probe 1, which includes the entire intergenic region between ORFs VP1722 (*ectA*) and VP1723 (Fig. 3B). This suggests direct regulation by OpaR. The 323-bp P*ectA* probe 1, which includes the first 33-bp of the *ectA* gene and 290-bp of the upstream regulatory region, was then divided into three smaller probes, P*ectA* 1A, 1B and 1C, and the EMSA was performed again with purified OpaR. OpaR bound to probe 1B indicating specificity of binding to the probe containing the putative OpaR binding site (Fig. 3C).

Bioinformatics analysis did not identify an AphA binding site within the intergenic region of VP1722 (*ectA*) and VP1723 (*bcct2* [this gene encodes betaine-carnitine-choline transporter 2]); however, a binding site was present within the coding region of VP1723 (Fig. 4A). EMSAs were performed using purified AphA protein, P*ectA* probe 1 (previously used in the OpaR P*ectA* EMSA) as a negative control (no putative binding site), and P*ectA* probe 2, which contained the putative AphA binding site (Fig. 4A). Probe 2

Downloaded from http://aem.asm.org/ on May 1, 2020 by guest

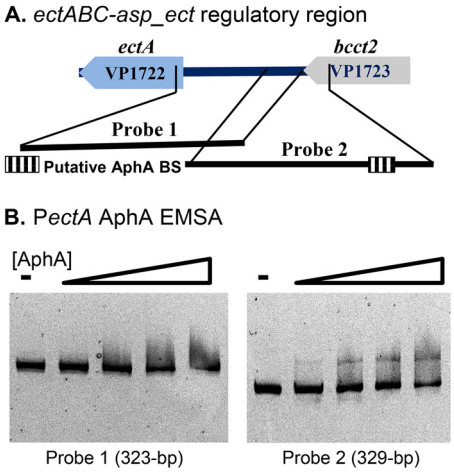

FIG 4 (A) The region upstream of *ectABC-asp_ect* (P*ectA*) is shown with a putative AphA binding site 441 bp upstream of the translational start, with P*ectA* probe 1 used in the OpaR EMSA and P*ectA* probe 2. P*ectA* probe 2 is 329 bp in length, contains the putative AphA binding site, and extends from 185 to 513 bp upstream of the ATG. (B) An EMSA was performed with 30 ng of P*ectA* probe 1 or probe 2 and purified AphA protein (0 to 0.84 μM) with DNA/protein molar ratios of 1:0, 1:15, 1:30, 1:45, and 1:60.

extends from 185 to 513 bp upstream of the ATG, overlapping with P*ectA* probe 1 by 106 bp. AphA bound to P*ectA* probe 2 (Fig. 4B), which indicates that the location of AphA binding is within the coding region of VP1723.

OpaR and AphA directly regulate the transcription of *ectABC-asp_ect*. Since AphA and OpaR bind directly to the upstream region of the *ectABC-asp_ect* operon, we next measured direct transcriptional regulation by both OpaR and AphA by using a GFP reporter assay in *Escherichia coli*. We expressed *opaR* or *aphA* from an expression plasmid (p*opaR* or p*aphA*), along with the P_{ectA}-*gfp* reporter plasmid in *E. coli* MKH13. *E. coli* lacks the *V. parahaemolyticus* quorum sensing components; therefore, expressing *opaR* or *aphA* in this background will determine the direct effects of each regulator on transcription of *ectABC-asp_ect*. The specific fluorescence was determined after overnight growth and compared to the specific fluorescence of a control strain harboring an empty expression vector (pBBR1MCS) and the P_{ectA}-*gfp* reporter. P_{ectA}-*gfp* activity in the *opaR*-expressing strain was significantly higher than the empty vector strain (Fig. 5A), indicating that OpaR activates transcription of these genes in *E. coli*. The total P_{ectA}-*gfp* activity in the *aphA*-expressing strain was significantly lower than that of the empty vector strain (Fig. 5B), suggesting that AphA acts as a repressor of the ectoine operon in an *E. coli* background. These data are in contrast to the *in vivo* P_{ectA}-*gfp* reporter data (Fig. 2A), which show that OpaR is a negative regulator and that AphA is

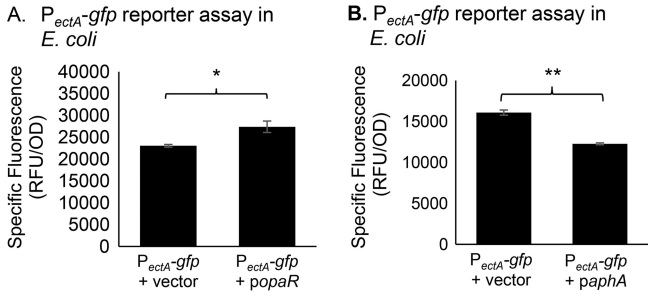

FIG 5 *E. coli* strain MKH13 harboring P_{ectA}-*gfp* and expression plasmid pBBR1MCS containing *opaR* (A) or *aphA* (B) under the control of an IPTG-inducible promoter (p*opaR* or p*aphA*). The fluorescence intensity and the OD were measured after overnight growth in M9G1% and compared to a strain with an empty expression vector. Two biological replicates are shown. Statistics were calculated using a Student *t* test (*, $P < 0.05$; **, $P < 0.01$).

Downloaded from http://aem.asm.org/ on May 1, 2020 by guest

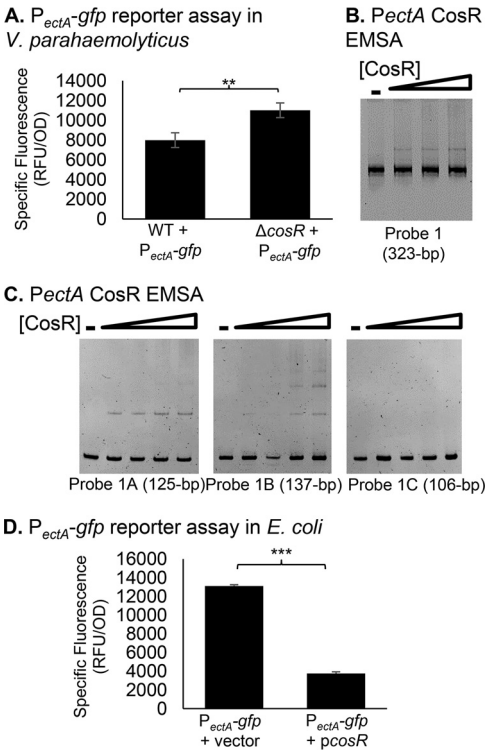

FIG 6 (A) A P_{ectA}-*gfp* reporter assay in WT *V. parahaemolyticus* and the Δ*cosR* mutant. Cultures were grown overnight in M9G3%, and the specific fluorescence was determined. Means and standard deviations of three biological replicates are shown. Statistics were calculated using a Student *t* test (**, $P < 0.01$; ***, $P < 0.001$). (B) An EMSA was performed with 30 ng of the full-length P*ectA* probe 1 and purified CosR protein (0 to 0.27 μM), with DNA/protein molar ratios of 1:0, 1:5, 1:10, and 1:20. (C) An EMSA was performed with 30 ng of each P*ectA* probe 1A, 1B, or 1C and purified CosR protein (0 to 0.65 μM), with DNA/protein molar ratios of 1:0, 1:1, 1:5, 1:10, and 1:15. (D) P_{ectA}-*gfp* reporter assay in *E. coli* strain MKH13 containing expression plasmid pBBR1MCS with *cosR* under the control of an IPTG-inducible promoter (p*cosR*). Cultures were induced and grown overnight in M9G1%. The specific fluorescence of the CosR-expressing strain was compared to a strain harboring empty pBBR1MCS. Means and standard deviations of at three biological replicates are shown. Statistics were calculated using a Student *t* test (***, $P < 0.001$).

a positive regulator of the ectoine operon. Since OpaR and AphA reciprocally repress each other and each regulate the *qrr* sRNAs, the absence of these additional regulatory mechanisms in *E. coli* likely contributes to the differences between the *V. parahaemolyticus in vivo* data and the *E. coli* reporter assays.

CosR is a repressor that binds directly to the *ectABC-asp_ect* regulatory region. Local regulators, CosR in *V. cholerae* and a homologue EctR1, in *M. alcaliphilum*, act as repressors of ectoine biosynthesis genes (14, 15). *Vibrio parahaemolyticus* encodes a homologue of $CosR_{Vc}$ encoded by VP1906 in strain RIMD2210633. $CosR_{Vc}$ and $CosR_{Vp}$ share 70% amino acid identity. Regulation of ectoine biosynthesis genes by CosR has not been investigated in *V. parahaemolyticus*. We determined whether CosR represses transcription of the *ect* operon by first constructing an in-frame deletion mutant of *cosR*. We then introduced the P_{ectA}-*gfp* reporter plasmid into the Δ*cosR* mutant and compared the reporter activity levels to that of the WT harboring P_{ectA}-*gfp* after growth in M9G3%. The P_{ectA}-*gfp* activity in the Δ*cosR* mutant strain was significantly higher than in the WT strain, indicating that CosR is a repressor (Fig. 6A).

To determine whether regulation of the *ect* operon by CosR is direct, we purified CosR with a C-terminal hexahistidine tag. We first performed an EMSA with the full-length P*ectA* probe 1, utilized previously in the OpaR EMSA, and various molar ratios of purified CosR. CosR bound to the P*ectA* probe 1 (Fig. 6B). A CosR consensus binding sequence is not available for *V. parahaemolyticus*, so we utilized the probes from our OpaR binding assay to narrow down potential binding sites and demonstrate the

Downloaded from http://aem.asm.org/ on May 1, 2020 by guest

specificity of the binding (Fig. 3A). EMSAs using these DNA probes were performed with various molar ratios of DNA probe to CosR. CosR bound specifically to probe 1A and probe 1B of the regulatory region (Fig. 6C), indicating that CosR is a direct regulator of this operon. CosR did not bind to probe 1C, demonstrating the binding specificity of CosR (Fig. 6C).

A GFP reporter assay in *E. coli* was utilized to determine the effect CosR has on transcription of the *ectABC-asp_ect* operon by measuring the transcriptional activity. The assay used *E. coli* strain MKH13 harboring two plasmids: an expression plasmid with full-length *cosR* under the control of an inducible promoter (p*cosR*) and a P_{ectA}-*gfp* reporter plasmid. Performing this reporter assay in *E. coli* allowed us to assess the contribution of CosR to transcription at the *ectABC-asp_ect* promoter in the absence of other *V. parahaemolyticus* proteins that may affect transcriptional regulation. The relative fluorescence and the OD were measured after growth in M9G1%. Specific fluorescence values were compared to a strain with an empty expression vector (pBBR1MCS). P_{ectA}-*gfp* reporter activity in the strain expressing CosR was 3.49-fold than in the empty-vector strain, indicating that CosR directly significantly represses transcription of the *ectABC-asp_ect* operon (Fig. 6D).

CosR is activated by OpaR and AphA. We utilized a GFP reporter assay to investigate whether CosR is under the control of the quorum sensing master regulator OpaR. We constructed a P_{cosR}-*gfp* reporter plasmid and introduced this into the WT strain and the Δ*opaR* mutant strain to measure transcriptional activity. The relative fluorescence and OD were measured after growth in M9G3%. The P_{cosR}-*gfp* reporter activity was significantly lower in the Δ*opaR* mutant strain than in the WT strain, indicating that OpaR is a positive regulator of the *cosR* gene (Fig. 7A).

Bioinformatics analysis identified one putative OpaR binding site in the regulatory region of the *cosR* gene, located 180 to 199 bp upstream of the translation start (Fig. 7B). We performed an EMSA with purified OpaR protein and two DNA probes comprising the upstream portion of the *cosR* regulatory region containing the putative binding site, and the region proximal to, and including, the ATG as a negative control (Fig. 7B). OpaR bound directly to P*cosR* probe A, but not to P*cosR* probe B (Fig. 7C). This indicates that OpaR is a direct regulator of *cosR* that binds specifically to probe A of the *cosR* regulatory region.

To demonstrate that direct binding of OpaR to the *cosR* regulatory region activates transcription, a reporter assay was performed in *E. coli* MKH13 harboring P_{cosR}-*gfp* and an expression vector harboring *opaR* under the control of an IPTG (isopropyl-β-D-thiogalactopyranoside)-inducible promoter. The specific fluorescence was calculated after growth in M9G1% and compared to a strain harboring an empty expression vector, along with the P_{cosR}-*gfp* reporter. In the OpaR-expressing strain, the P_{cosR}-*gfp* reporter activity was significantly higher than in the empty vector strain, indicating that OpaR directly activates the transcription of *cosR* (Fig. 7D).

We next determined whether AphA regulates transcription of *cosR*. Utilizing our P_{cosR}-*gfp* reporter plasmid, we assessed P_{cosR}-*gfp* activity in the WT and Δ*aphA* strains. The relative fluorescence and OD were measured after growth in M9G3%. The P_{cosR}-*gfp* reporter activity was significantly lower in the Δ*aphA* mutant strain than in the WT strain, indicating that AphA is a positive regulator of the *cosR* gene (Fig. 8A). Using bioinformatics analysis, we identified a putative AphA binding site in the *cosR* regulatory region (Fig. 8B). An EMSA was performed with probe A (188 bp) containing the putative binding site and probe B (142 bp) with no binding site. In this assay, AphA did not bind to either probe (Fig. 8C). This suggests that AphA does not directly regulate *cosR* or that AphA requires an additional factor to bind.

Quorum sensing regulation of ectoine biosynthesis genes in *Vibrionaceae*. The ability to biosynthesize ectoine is phylogenetically widespread among the *Vibrionaceae* family (5). It was determined previously through mutational analyses that three residues—I24, A51, and T52—within the DNA-binding domains of LuxR are important for repression of target genes in *V. harveyi* ATCC BAA-1116 (30). We determined that

Downloaded from http://aem.asm.org/ on May 1, 2020 by guest

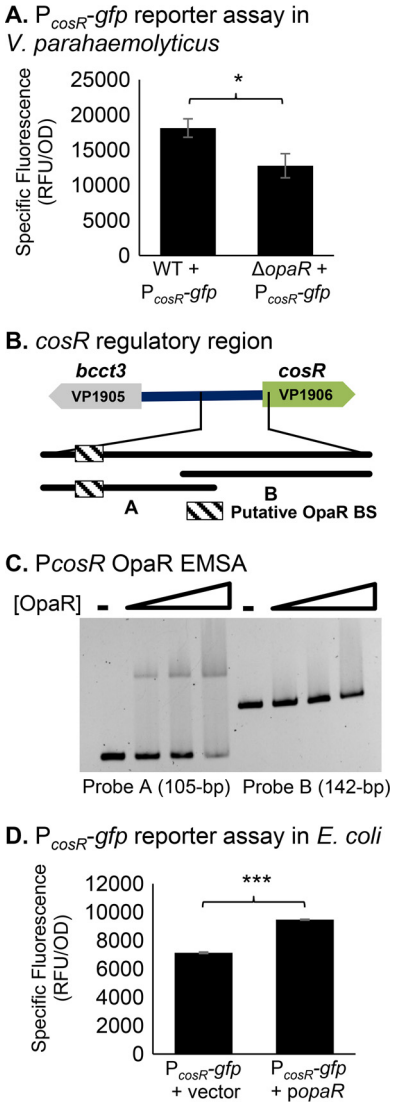

FIG 7 (A) A P$_{cosR}$-*gfp* reporter assay in WT *V. parahaemolyticus* and the Δ*opaR* mutant harboring a P$_{cosR}$-*gfp* transcriptional fusion reporter plasmid. Cultures were grown overnight in M9G3%, and the specific fluorescence was determined by dividing the RFU by the OD. Means and standard deviations of at three biological replicates are shown. Statistics were calculated using a Student *t* test (*, $P < 0.05$) (B) A 224-bp region of the *cosR* regulatory region (P*cosR*; positions +4 to −220 relative to ATG) was divided into two similarly sized probes A and B (105p and 142 bp in length, respectively). A putative OpaR binding site is located 180 to 199 bp upstream of the translation start, within probe A. (C) An EMSA was performed with various concentrations of purified OpaR protein (0 to 0.88 μM) and P*cosR* probe A or B. Each lane contains 30 ng of DNA probe, with molar DNA/protein ratios of 1:0, 1:1, 1:10, and 1:20. (D) *E. coli* strain MKH13 harboring P$_{cosR}$-*gfp* and expression plasmid pBBR1MCS containing *opaR* under the control of an IPTG-inducible promoter (p*opaR*). Cultures were induced and grown overnight in M9G1%. The specific fluorescence of the OpaR-expressing strain was compared to a strain harboring empty expression vector. Means and standard deviations of two biological replicates are shown. Statistics were calculated using a Student *t* test (***, $P < 0.001$).

homologues of LuxR in multiple *Vibrio* species also contained these conserved amino acids and therefore likely bind to target genes in the same manner (data not shown). We used the OpaR consensus binding motif to predict binding sites in the regulatory region of the ectoine biosynthesis genes in multiple *Vibrio* species. Putative binding sites, along with distance from the ATG, the log odds score, the probability of binding, and a given *P* value, are listed in Table 1. Only binding sites that were returned with a probability of ≥90% are shown. The probability of a LuxR-type binding site in *V. alginolyticus*, the most closely related species to *V. parahaemolyticus* is 99.1%, and the

Downloaded from http://aem.asm.org/ on May 1, 2020 by guest

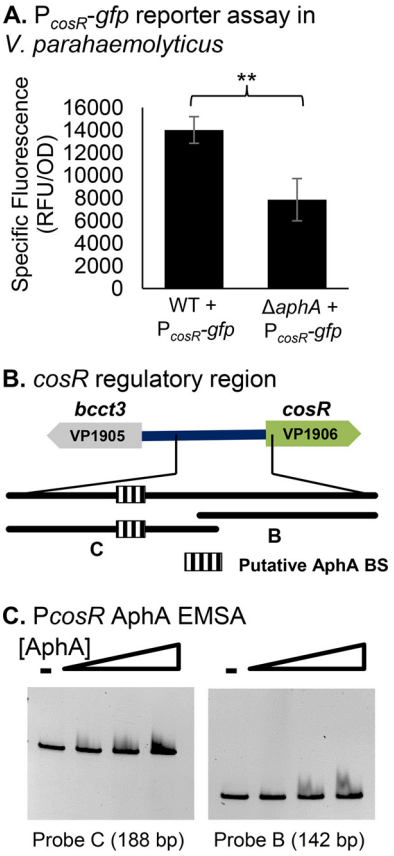

FIG 8 (A) A P_{cosR}-*gfp* reporter assay in wild-type (WT) *V. parahaemolyticus* and the Δ*aphA* mutant harboring a P_{cosR}-*gfp* transcriptional fusion reporter plasmid. Cultures were grown overnight in M9G3%, and the specific fluorescence was determined by dividing the RFU by the OD. Means and standard deviations of three biological replicates are shown. Statistics were calculated using a Student *t* test (**, $P < 0.01$). (B) The regulatory region of the *cosR* gene (positions +4 to −327 relative to the ATG) was divided into two similarly sized probes: probe B, used previously in the OpaR EMSA, and probe C (142 and 188 bp in length, respectively). A putative AphA binding site is located 204 to 223 bp upstream of the ATG, within probe C. (C) An EMSA was performed with various concentrations of purified AphA protein (0 to 0.88 μM) and P*cosR* probe B or probe C. Each lane contains 30 ng of DNA probe and DNA/protein molar ratios of 1:0, 1:15, 1:30, and 1:45.

probabilities are 95% in *V. harveyi* 1DA3 in ATCC BAA-1116 and 92% in *V. splendidus*; each strain has one predicted binding site. Several species have multiple predicted binding sites. Overall, these data suggest that quorum sensing control of the ectoine biosynthesis system is likely widespread among *Vibrio* species.

DISCUSSION

In this study, we investigated regulation of the ectoine biosynthesis operon by the quorum sensing regulators AphA and OpaR. Ectoine genes are most highly expressed in the early exponential phase, and levels fall concurrently with AphA levels. This ensures that adequate transcripts are present to produce the enzymes necessary for the conversion of aspartic acid to ectoine during the exponential phase, when the cells are rapidly growing and dividing. We found that expression of the *ectABC-asp_ect* operon is activated by AphA and repressed by OpaR. This suggests that OpaR represses expression during the late exponential phase when the requirement for ectoine production begins to diminish, as the cells approach stationary phase and are no longer replicating. In addition, we show that AphA and OpaR activate transcription of CosR, which also represses *ectABC-asp_ect*. In this transcriptional motif, a feed-forward loop, a general transcription factor (OpaR or AphA) controls a specific transcription factor (CosR), and both transcription factors regulate the output of the effector operon

Downloaded from http://aem.asm.org/ on May 1, 2020 by guest

TABLE 1 Putative OpaR binding sites in the ectoine regulatory region of *Vibrio* species[a]

Species	Binding site	Upstream ATG size (bp)	Log odds score	*P* (binding)	*P* (given)	Strain accession no.
V. parahaemolyticus	AAATGATGCTTTAATAAATT	147	3.69	0.976	0.003	GCA_000196095.1
V. alginolyticus	TAGGTGACTATTTAATAAAT	179	4.65	0.991	0.005	GCA_000354175.2
V. harveyi 1DA3	CAATTTATTTTTCACCCTAT	155	2.96	0.951	0.005	GCA_000182685.1
V. harveyi ATCC BAA-1116	CGATTAATTTTTTACCCTAT	187	3.03	0.954	0.005	GCA_000017705.1
V. splendidus	CAAAGTATTATTTAATACAT	129	2.46	0.921	0.005	GCA_003049855.1
V. brasiliensis	CTGCTGACATTAATTAGAGT	330	2.24	0.904	0.005	GCF_000189255.1
	TTAATTAGAGTTCTAACTAA	321	3.19	0.961	0.0025	
	GTATTGTTTCTAAGGACTAA	211	2.48	0.923	0.005	
	TTATTGAGTAAACCTTTAGT	150	5.69	0.997	0.0005	
	CTTTAGTTTTAACTCTAAAT	137	4.43	0.988	0.001	
	ATAATGAATGTGAAATTTGT	16	4.50	0.989	0.001	
V. orientalis	TTTTTATTTGTACTCTAATT	386	2.22	0.902	0.005	GCA_000176235.1
	TAATTAATAAATCGCATTAT	371	5.67	0.997	0.0005	
	ATTAAATTAAATTGGTTAAT	322	3.13	0.958	0.0025	
	AATTGGTTAATTTAGCATTA	313	4.41	0.988	0.001	
	CAAATGGCTAATCATTAAGT	283	2.39	0.916	0.005	
V. anguillarum	AATTGTGAACAAAGAGTATT	417	2.25	0.904	0.005	GCA_000217675.1
	TTATATAGAGATTTTTAATT	36	2.50	0.924	0.005	
	ATATAGAGATTTTTAATTAG	34	2.16	0.897	0.005	
	TTAATTAGAGCTCTAACTAT	22	4.06	0.983	0.005	
V. furnissii	ATATAGTGTGAACAAAATGT	427	2.35	0.914	0.005	GCA_000184325.1
	CTAGTGATAGCAATGTAACT	217	3.42	0.968	0.0025	
	GGTTTTATTGAATTATCCAT	87	2.85	0.946	0.005	
	TTATTGAATTATCCATTATT	83	4.58	0.990	0.001	
V. mimicus	GTAAAAATAGAAATATGATT	43	4.59	0.990	0.001	GCA_001767355.1
V. parahaemolyticus (upstream of *opaR*)[b]	TAATGACATTACTGTCTATA	127	9.94	1.00	0.00001	

[a]The probability of binding and the given *P* value are both indicated.
[b]The binding site of OpaR to its own promoter is included here for comparison.

(*ectABC-asp_ect*). This regulation scheme presumably results in precise control of energetically costly ectoine production across the growth cycle (Fig. 9). The complexity of regulation of the *ectABC-asp_ect* operon likely explains the conflicting results of our *V. parahaemolyticus in vivo* and *E. coli* reporter assays. Here, we have shown that at least three regulators are involved in direct transcriptional control of the *ect* genes. Control by each regulator is more than likely affected by the other regulators. This could occur

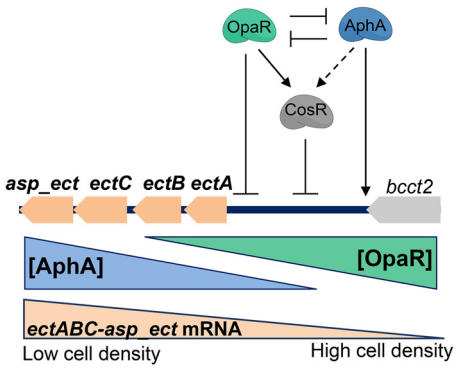

FIG 9 Model of ectoine biosynthesis gene regulation by quorum sensing regulators. The dashed line indicates indirect regulation, while solid lines indicate direct regulation. AphA is activated at a low cell density and activates the transcription of *ectABC-asp_ect*. OpaR is activated during the transition from a low cell density to a high cell density. As levels of OpaR increase, the levels of AphA decrease, and OpaR represses *ectABC-asp_ect* transcription. OpaR and AphA activate transcription of *cosR*. CosR participates in a feed-forward loop to repress *ectABC-asp_ect* transcription. This regulatory loop produces a gradient of *ectABC-asp_ect* transcripts across the growth cycle.

Downloaded from http://aem.asm.org/ on May 1, 2020 by guest

either via direct interactions at the regulatory region or indirectly via transcriptional control of each other, as OpaR and AphA reciprocally repress each other and both activate CosR. In addition, given the complexity of the quorum sensing regulatory circuit, it is probable that other regulators play a role in fine-tuning ectoine production via transcriptional, posttranscriptional, and enzyme-level regulation of ectoine biosynthesis. Due to an associated energy cost (34), it is reasonable that bacteria would utilize multiple levels of regulation to tightly control ectoine production in the cell.

The physiology of *V. parahaemolyticus* provides one explanation for quorum sensing control of ectoine production. In order to reach a high cell density, *V. parahaemolyticus* grows optimally in high salinity, which requires the accumulation of compatible solutes. Therefore, integration of quorum sensing regulators with osmotic tolerance would allow *V. parahaemolyticus* to respond to environmental stressors and to maximize production of compatible solutes at both low and high cell densities. Quorum sensing has been linked with multiple stress responses in bacteria. In *V. cholerae*, it was shown that HapR (LuxR homologue) activates *rpoS*, the general stress response sigma factor, increasing survival under environmental stress (35). A study in *Burkholderia glumae* revealed that quorum sensing functions to maintain bacterial osmolality by negatively regulating glutamate uptake and nitrogen metabolism (36). In *V. harveyi*, a species closely related to *V. parahaemolyticus*, the quorum sensing master regulator LuxR was shown to directly regulate the transcription of the glycine betaine biosynthesis operon (32).

Vibrio spp. thrive in warmer temperatures and increased salinity and cause infections mostly in the warmer months of the year. High salinity enables *V. parahaemolyticus* to adapt to other abiotic stresses, such as temperature (37, 38). This, along with warming ocean temperatures, has facilitated the expansion of the range of *V. parahaemolyticus* as far north as Alaska (39), with infection rates in the United States increasing over the last several years (40). *V. parahaemolyticus* poses a growing threat to the shellfish industry, where despite strict guidelines for handling, high incidence rates persist (41, 42). The present study furthers the understanding of osmotic stress response regulation in *V. parahaemolyticus* and is an important step in understanding increased *Vibrio* proliferation in warmer ocean temperatures when salinity is elevated.

MATERIALS AND METHODS

Bacterial strains, media, and culture conditions. All strains and plasmids used in this study are listed in Table 2. A previously described streptomycin-resistant clinical isolate of *V. parahaemolyticus* RIMD2210633 was used as the wild-type (WT) strain (43). Strains were grown in either lysogeny broth (LB; Fisher Scientific, Fair Lawn, NJ) supplemented with 3% (wt/vol) NaCl (LBS) or in M9 minimal medium (47.8 mM Na_2HPO_4, 22 mM KH_2PO_4, 18.7 mM NH_4Cl, 8.6 mM NaCl; Sigma-Aldrich) supplemented with 2 mM $MgSO_4$, 0.1 mM $CaCl_2$, and 20 mM glucose as the sole carbon source (M9G), and either 3 or 6% (wt/vol) NaCl (M9G3% or M9G6%). *E. coli* strains were grown in LB supplemented with 1% (wt/vol) NaCl (LB1%) or M9G supplemented with 1% NaCl (M9G1%) where indicated. *E. coli* β2155 λ*pir*, a diaminopimelic acid (DAP) auxotroph, was supplemented with 0.3 mM DAP and grown in LB1%. All strains were grown at 37°C with aeration. Antibiotics were used at the following concentrations (wt/vol) as necessary: ampicillin (Amp), 50 μg/ml; chloramphenicol (Cm), 12.5 μg/ml; streptomycin (Str), 200 μg/ml; and tetracycline (Tet), 1 μg/ml. Ectoine was added to media to a final concentration of 100 μM, when indicated.

Construction of the *cosR* deletion mutant. A Gibson assembly protocol, using NEBuilder HiFi DNA assembly master mix (New England Biolabs, Ipswich, MA) was used to generate an in-frame truncated, nonfunctional *cosR* gene in the suicide vector pDS132 (pDSΔ*cosR*), followed by allelic exchange (44, 45). Primers pairs were designed to create a 60-bp truncated PCR product of the 477-bp *cosR* gene (Table 3). PCR amplification, using genomic DNA from *V. parahaemolyticus* RIMD2210633 as the template and the primer sets SOEcosRA/SOEcosRB and SOEcosRC/SOEcosRD, was performed to produce two fragments, AB and CD, of the *cosR* gene. Complementary regions for Gibson assembly are indicated in lowercase letters in the primer sequences in Table 3. AB and CD fragments were ligated with pDS132 vector linearized with SacI via Gibson assembly to generate pDSΔ*cosR*. pDS132 harboring the truncated version of *cosR*, which was transformed into the *E. coli* strain β2155 λ*pir*, followed by conjugation into *V. parahaemolyticus*. For the pDSΔ*cosR* suicide vector to be maintained in the cell, the vector undergoes homologous recombination into the genome, since *V. parahaemolyticus* does not contain the *pir* gene required for replication of the pDSΔ*cosR* plasmid. Positive colonies were selected on chloramphenicol plates to contain a single crossover of pDSΔ*cosR* in the genome. A culture was grown overnight in the absence of chloramphenicol to induce a second recombination event, leaving behind either the truncated mutant *cosR* allele or the WT allele in the genome. Colonies were plated on sucrose for selection. Colonies of cells that still contain the plasmid appeared soupy on the sucrose plate due to the presence of the *sacB* gene on the pDSΔ*cosR*

Downloaded from http://aem.asm.org/ on May 1, 2020 by guest

TABLE 2 Strains and plasmids used in this study

Strain or plasmid	Genotype[a]	Source or reference(s)
Strains		
Vibrio parahaemolyticus		
RIMD2210633	O3:K6 clinical isolate; Str^r	37, 43
SSK2099 (Δ*luxO*)	RIMD2210633 Δ*luxO* (VP2099); Str^r	22
SSK2516 (Δ*opaR*)	RIMD2210633 Δ*opaR* (VP2516); Str^r	22
SSK2762 (Δ*aphA*)	RIMD2210633 Δ*aphA* (VP2762); Str^r	22
SSK9916 (Δ*luxO* Δ*opaR*)	RIMD2210633 Δ*luxO* Δ*opaR*; Str^r	22
SSK1662 (Δ*opaR* Δ*aphA*)	RIMD2210633 Δ*opaR* Δ*aphA*; Str^r	22
Δ*cosR* mutant	RIMD2210633 Δ*cosR* (VP1906); Str^r	This study
Escherichia coli		
DH5α λ*pir* mutant	Δ*lac pir*	Thermo Fisher Scientific
β2155 λ*pir* mutant	Δ*dapA*::*erm pir* for bacterial conjugation	49
BL21(DE3)	Expression strain	Thermo Fisher Scientific
MKH13	MC4100 (Δ*betTIBA*) Δ(*putPA*)*101* Δ(*proP*)*2* Δ(*proU*); Sp^r	48
Plasmids		
pDS132	Suicide plasmid; Cm^r; *sacB* (sucrose intolerant), R6Kg origin	50
pDSΔ*cosR*	pDS132 harbording truncated *cosR* allele	This study
pBBR1MCS	Empty expression vector, *lacZ* promoter; Cm^r; pBBR1 origin	51
pBBR*opaR*	pBBR1MCS harboring full-length *opaR* (VP2516)	This study
pBBR*cosR*	pBBR1MCS harboring full-length *cosR* (VP1906)	This study
pBBR*aphA*	pBBR1MCS harboring full-length *aphA* (VP2762)	This study
pRU1064	Promoterless-*gfp*UV; Amp^r Tet^r; IncP origin	47
pRUP*ectA*	pRU1064 with P*ectA-gfp*, Amp^r Tet^r	This study
pRUP*cosR*	pRU1064 with P*cosR-gfp*, Amp^r Tet^r	This study
pMAL-c5x	Empty expression vector, TEV site; Amp^r	52
pMAL*aphA*	pMAL harboring *aphA*; Amp^r	This study
pET28a+	Empty expression vector, 6×His; Kan^r	Novagen
pET*cosR*	Pet28a+ harboring *cosR*; Kan^r	This study

[a]Cm^r, chloramphenicol resistance; Tet^r, tetracycline resistance; Amp^r, ampicillin resistance; Sp^r, spectinomycin resistance; Str^r, streptomycin resistance.

plasmid. Colonies were screened via PCR assays for the presence of a mutant allele. Positive colonies were sequenced to confirm an in-frame deletion of the *cosR* gene.

RNA isolation and quantitative real-time PCR. *Vibrio parahaemolyticus* RIMD2210633 was grown overnight at 37°C with aeration in LBS. Cells were then washed two times with 1× phosphate-buffered saline (PBS), diluted 1:50 into 50 ml of M9G3%, and grown with aeration at 37°C. Cells were harvested at an OD_{595} of 0.15, 0.25, 0.4, 0.5, 0.8, or 1.0. For the 0.15 OD sample, RNA was isolated from 5 ml of culture. For all other samples, RNA was isolated from 1 ml of culture. according to the manufacturer's protocol, total RNA was extracted using TRIzol (Invitrogen, Carlsbad, CA). The concentrations of RNA were determined using a NanoDrop spectrophotometer (Thermo Scientific, Waltham, MA). The samples were then treated with Turbo DNase (Invitrogen). Superscript IV reverse transcriptase (Invitrogen) was used to synthesize cDNA from 500 ng of RNA by priming with random hexamers. cDNA samples were then diluted 1:25, and quantitative real-time PCR (qPCR) was performed using cDNA. PowerUp SYBR green master mix (Life Technologies) was used, and samples were run on an Applied Biosystems QuantStudio6 fast real-time PCR system (Applied Biosystems, Foster City, CA). Reactions were set up with the following primer pairs: 16SFwd/Rev, for normalization, ectAFwd/Rev, asp-ectFwd/Rev, aphAFwd/Rev, and opaR-Fwd/Rev (Table 3). The qPCR primer efficiency was determined for each primer pair using a standard curve. The efficiency of each pair was as follows: *opaR*, 101.96%; *aphA*, 102.81%; *ectA*, 98.09%; *asp_ect*, 98.73%; and 16S, 95.99%. Cycle threshold (C_T) values were used to determine expression levels, and all samples were normalized to 16S rRNA. Expression levels were calculated relative to the OD_{595} 0.15 sample, using the $\Delta\Delta C_T$ method, as described previously (46).

Protein purification of AphA, OpaR, and CosR. *Vibrio parahaemolyticus* RIMD2210633 OpaR was purified as previously described (22). The 540-bp *aphA* (VP2762) gene was cloned into a pMAL-c5x vector with a hexahistidine-tagged maltose-binding protein tag and TEV protease cleavage site upstream of the multiple-cloning site. Full-length *aphA* was amplified from *V. parahaemolyticus* RIMD2210633 genomic DNA using the primer pair NcoIaphAFwd/BamHIaphARev, which included restriction cut sites in the 5′ end of the primers (Table 3). The pMAL vector and the purified PCR fragment were digested with NcoI and BamHI and ligated with T4 ligase (Invitrogen). The pMAL*aphA* plasmid was transformed into *E. coli* Dh5α, purified, and sequenced. The pMAL*aphA* plasmid was then transformed into *E. coli* BL21(DE3) cells. MBP-AphA was then expressed and purified. Portions (10 ml) of overnight culture were used to inoculate 1 liter of LB supplemented with 0.2% glucose at 37°C. This culture was induced with 0.5 mM IPTG at OD_{595} 0.5. Growth continued overnight at 18°C. Cells were harvested by centrifugation (5,000 × *g* for 20 min at 4°C) and resuspended in amylose column buffer (50 mM sodium phosphate, 200 mM NaCl [pH 7.5]) supplemented with 1 mM phenylmethanesulfonyl fluoride and 0.5 mM benzamidine. Bacterial cells were lysed on ice using a high-pressure homogenizer (EmulsiFlex-C5; Avestin, Ottawa, Canada). Cell debris was removed by centrifugation (15,000 × *g* for 1 h at 4°C). The supernatant was diluted 1:6 with

Downloaded from http://aem.asm.org/ on May 1, 2020 by guest

TABLE 3 Primers used in this study

Analysis and primer	Sequence (5′–3′)[a]	Length (bp)
Mutant		
SOEVPcosRA	accgcatgcgatatcgagctTCAAAGCCCCACTTTTGAAC	511
SOEVPcosRB	tgatgctgccgatAATCGAGACCAATACTTCTTCG	
SOEVPcosRC	ggtctcgattATCGGCAGCATCACCAAAC	522
SOEVPcosRD	gtggaattcccgggagagctCAATCATGAATGGCATCG	
SOEVPcosRFLFwd	CCCATCCAATGCTGTCTTCG	1,838
SOEVPcosRFLRev	CATGCAAGAACGTGTGGAGT	
Protein expression		
NcoIaphAFwd	TGCCCATGGGAATGTCATTACCACACGTAATC	540
BamHIaphARev	CTCGGATCCTTAACCAATCACTTCAAGTTCTGTTAGG	
NcoIcosRFwd	TACGGCGCCATGGACTCAATTGCAAAGAG	625
XhoIcosRRev	CACGAGCTCTTAGTGTTCGCGATTGTAGA	
EMSA		
VPectAFwd1A	CCAAGGTGCTGATGTGATCA	125
VPectARev1A	CACATTAATCCAGATTAAAACGCAG	
VPectAFwd1B	CTGCGTTTTAATCTGGATTAATGTG	137
VPectARev1B	CCCACTGCATTCTGACTCAT	
VPectAFwd1C	TGAGTCAGAATGCAGTGGG	106
VPectARev1C	GCCACGACGACAAAACTAAC	
VPectARev2	GTAAAGTCGATGCGCCAACAC	
VPcosRFwdA	CAAATCTCCACACCATTAATTAG	105
VPcosRRevA	CGTCTTTGGTGATTTCTTTTTATTCGC	
VPcosRFwdB	GCGAATAAAAAGAAATCACCAAAGACG	142
VPcosRRevB	CCAATTTTTTCATCCAGTCTGTAGGG	
VPcosRFwdC	CCCGTGAAAGCGGAAGATC	188
VPcosRRevC	CGCTCGTGCAACTGAAACA	
Expression		
opaRCFwd	agggaacaaaagctgggtacAATGGCAAGGAAAATGGATATG	642
opaRCRev	cggccgctctagaactagtgGGGCTTGTTCGTGTTCAAATC	
cosRCFwd	agggaacaaaagctgggtacTTCCCTACAGACTGGATG	501
cosRCRev	cggccgctctagaactagtgTTATTCTGGTTTGGTGATG	
aphACFwd	agggaacaaaagctgggtacGACCATTTGGATTGAAGAC	559
aphACRev	cggccgctctagaactagtgTTAACCAATCACTTCAAGTTC	
GFP reporter		
PectAPFwd	CTCAAGCTTGTAAAGTCGATGCGCCAAC	514
PectAPRev	TATACTAGTATCCTTTGACGTCTAATTAAATTTC	
PcosRPFwd	tagatagagagagagagagaCGTTCCTCTCTATTTTTGTATTATTTTTTC	397
PcosRPRev	actcatttttttcttcctccaAATTTTTTCATCCAGTCTGTAGG	
qPCR		
opaRFwd	CCATGTTGTCCGTCAGTTCTCG	158
opaRRev	GAGTTGATGCGCTCCACTCG	
aphAFwd	AGCCACCAACAAGTTTACCG	140
aphARev	CATTCTCCAAGAGCGCTACG	
ectAFwd	CCAATGGCGGTTGTACTGCTGAAA	269
ectARev	TCACCGTGAATACACTCGATGCCA	
asp-ectFwd	CGATGATTCCATTCGCGACG	126
asp-ectRev	GTCATCTCACTGTAGCCCCG	
16SFwd	ACCGCCTGGGGAGTACGGTC	234
16SRev	TTGCGCTCGTTGCGGGACTT	

[a]Complementary regions for Gibson assembly are indicated in lowercase letters.

amylose column buffer and passed through a column containing 20 ml of amylose resin (New England BioLabs). The column was washed with 10 column volumes (CVs) of amylose wash buffer. The fusion protein, MBP-AphA, was eluted with three CVs amylose elution buffer (50 mM sodium phosphate, 200 mM NaCl, 20 mM maltose [pH 7.5]). After purification, the MBP tag was removed by overnight incubation of the eluent at 4°C with a hexahistidine-tagged tobacco etch virus (TEV) protease (a gift from Sharon Rozovsky, University of Delaware) in a 1:10 molar ratio. The cleavage mixture was then adjusted to 20 mM imidazole and subjected to immobilized metal affinity chromatography (IMAC) using HisPur Ni-NTA resin (Thermo Fisher) to remove the hexahistidine-tagged TEV protease, the hexahistidine-tagged MBP protein, and any uncleaved MBP-AphA. AphA was further purified using size exclusion chromatography by passage over a GE HiPrep Sephacryl S100 column and analyzed for purity by SDS-PAGE, and the molecular weight was confirmed using mass spectrometry.

Downloaded from http://aem.asm.org/ on May 1, 2020 by guest

The 477-bp *cosR* (VP1906) gene was cloned into pET-28a(+) (Novagen) with a C-terminal hexahistidine tag using the primer pair NcoIcosRFwd/XhoIcosRRev (Table 3). The pET28a(+) vector and the purified PCR fragment were digested with NcoI and XhoI and ligated via sticky-end ligation with T4 ligase (Invitrogen). The pET*cosR* plasmid was transformed into *E. coli* Dh5α, purified, and sequenced. The pET*cosR* plasmid was transformed into *E. coli* BL21(DE3) cells. CosR-His expression was induced with 0.5 mM IPTG at 0.4 OD_{595} and grown overnight with aeration at 25°C. The cells were then pelleted, resuspended in lysis buffer (50 mM sodium phosphate, 200 mM NaCl, 20 mM imidazole [pH 7.4], 1.0 mM phenylmethanesulfonyl fluoride, 0.5 mM benzamidine), and lysed using a microfluidizer. Debris was pelleted through centrifugation at 24,000 $\times$ *g* for 35 min at 4°C. Clarified supernatant was subjected to IMAC using a column packed with HisPur Ni-NTA resin (Thermo Fisher) and equilibrated with column buffer (50 mM sodium phosphate, 200 mM NaCl, 20 mM imidazole [pH 7.4]). The column was washed with 20 CVs of column buffer, 20 CVs of a buffer containing 40 mM imidazole, and 10 CVs of buffer containing 100 mM imidazole to remove any remaining contaminants. CosR-His was eluted using three CVs of 500 mM imidazole buffer. After elution, the samples dialyzed overnight at 4°C in sodium phosphate buffer to remove any excess salts. The protein purity was estimated at 95% using SDS-PAGE.

Electrophoretic mobility shift assay. Two overlapping DNA fragments designated P*ectA* probe 1 (323 bp) and probe 2 (329 bp) were amplified using the primer sets VPectAFwd1A/Rev1C and VPectAFwd1C/Rev2. Probe 1 was split into three similarly sized probes 1A (125 bp), 1B (137 bp), and 1C (106 bp). These probes were amplified using the primer sets VPectAFwd1A/Rev1A, VPectAFwd1B/Rev1B, and VPectAFwd1C/Rev1C (Table 3). Two overlapping DNA fragments, 105 and 142 bp, were amplified from *V. parahaemolyticus* RIMD2210633 using the primer sets VPcosRFwdA/VPcosRRevA and VPcosRFwdB/VPcosRRevB, comprising 220 bp of the *cosR* regulatory region. An additional probe, probe C, 188 bp in length, which contained a putative AphA binding site, was amplified using the primer set VPcosRCFwd/VPcosRCRev (Table 3). The protein concentration was determined using Bradford reagent. Various concentrations of purified OpaR, AphA, or CosR were incubated for 20 min with 30 ng of each DNA fragment in OpaR/CosR binding buffer (10 mM Tris, 150 mM KCl, 0.1 mM dithiothreitol, 0.1 mM EDTA, 5% polyethylene glycol [PEG]; pH 7.9 at 4°C) or AphA binding buffer (10 mM Tris, 150 mM KCl, 0.1 mM dithiothreitol, 0.1 mM EDTA, 5% PEG [pH 7.5 at 4°C]). A 6% native acrylamide gel was prerun for 2 h at 4°C (200 V) with Tris-acetate-EDTA (TAE) buffer (pH 8.4 for OpaR and CosR [pH 7.5] for AphA at 4°C). The DNA-protein mixtures (10 μl) were loaded onto the gel and run for 2 h at 4°C (200 V) in 1$\times$ TAE buffer. The gels were then stained for 20 min in an ethidium bromide bath (0.5 μg/ml).

Transcriptional reporter assays. GFP reporter plasmids were constructed by cloning the regulatory region of interest upstream of a promoterless *gfp* gene in the parent vector pRU1064, which contains both tetracycline and ampicillin resistance cassettes (47). The P*ectA* regulatory region was amplified from *V. parahaemolyticus* RIMD2210633 genomic DNA with the primer pairs listed in Table 3. The P*ectA* region encompasses 514 bp upstream of *ectA*, including 224 bp of the open reading frame coding region of VP1723. P*ectA* was cloned into pRU1064 via digestion with HindIII and SpeI and ligation with T4 ligase to produce the $pRUP_{ectA}$-*gfp* reporter plasmid. The P*cosR* regulatory region was amplified from *V. parahaemolyticus* RIMD2210633 genomic DNA using the primer pairs listed in Table 3, generating a 397-bp probe. pRU1064 was linearized with SpeI and ligated with P*cosR* via Gibson assembly protocol to produce the $pRUP_{cosR}$-*gfp* reporter plasmid (44). Complementary regions for Gibson assembly are indicated in lowercase letters in the primer sequence (Table 3). The plasmids were transformed into *E. coli* Dh5α, purified, and sequenced. The reporter plasmids were subsequently transformed into *E. coli* β2155 λ*pir* and conjugated into the WT and quorum sensing mutant strains. Wild-type and single-deletion mutants of each quorum sensing regulator (Δ*luxO*, Δ*opaR*, and Δ*aphA*), as well as the double-deletion mutants (Δ*luxO* Δ*opaR* and Δ*opaR* Δ*aphA*) containing $pRUP_{ectA}$-*gfp*, $pRUP_{cosR}$-*gfp* or the promoterless parent reporter vector pRU1064, were grown overnight in LB3% with tetracycline (1 μg/ml), washed twice with 1$\times$ PBS, and then diluted 1:100 into M9G3% media and grown for 20 h under tetracycline selection to an OD_{595} between 0.9 and 1.1. Reporter expression over the growth cycle was determined by measuring GFP fluorescence with excitation at 385 nm and emission at 509 nm in black, clear-bottom 96-well plates on a Tecan Spark microplate reader with Magellan software (Tecan Systems, Inc., San Jose, CA). The specific fluorescence was calculated for each sample by dividing the fluorescence intensity by the OD_{595}. Three biological replicates were performed for each experiment.

GFP reporter assays were conducted in the *E. coli* strain MKH13 [F *araD139* (*argF lac*)*U169 rpsL150 relA1 deoC1 ptsF25 rbsR flbB5301*] (48). A full-length copy of *opaR*, *cosR*, or *aphA* was cloned into the pBBR1MCS expression vector, which contains an IPTG-inducible promoter using the primer pairs opaRCFwd/opaRCRev, cosRCFwd/cosRCRev, and aphACFwd/aphACRev (Table 3). pBBR1MCS was linearized via digestion with KpnI and BamHI. Purified PCR fragments were ligated with linearized pBBR1MCS via the Gibson assembly protocol to generate pBBR*opaR*, pBBR*cosR*, or pBBR*aphA*. Complementary regions for Gibson assembly are indicated in lowercase letters in the primer sequences in Table 3. The plasmids were transformed into *E. coli* Dh5α, purified, and sequenced. The purified plasmids, along with empty pBBR1MCS expression vector, were transformed into *E. coli* strain MKH13. The reporter plasmids $pRUP_{ectA}$-*gfp* and $pRUP_{cosR}$-*gfp* were then transformed into the MKH13 strains containing pBBR*opaR*, pBBR*cosR*, pBBR*aphA*, or pBBR1MCS empty vector. Strains containing the $pRUP_{ectA}$-*gfp* reporter plasmid and pBBR*cosR* were grown overnight in LB1% with ampicillin (25 μg/ml) and chloramphenicol (12.5 μg/ml), washed twice with 1$\times$ PBS, and diluted 1:1,000 into M9G1%. pBBR*cosR* was then induced with 250 μM IPTG, and strains were grown overnight under antibiotic selection to an OD_{595} between 0.9 and 1.1. Strains containing the $pRUP_{cosR}$-*gfp* reporter plasmid and pBBR*opaR* or pBBR*aphA* were grown overnight in LB1% with ampicillin (25 μg/ml) and chloramphenicol (12.5 μg/ml), washed twice with 1$\times$ PBS, and diluted 1:50 into M9G1%. pBBR*opaR* or pBBR*aphA* was then induced with 10 μM IPTG, and

Downloaded from http://aem.asm.org/ on May 1, 2020 by guest

strains were grown for 20 h under antibiotic selection to an OD_{595} between 0.9 and 1.1. Reporter expression was determined by measuring the GFP fluorescence with excitation at 385 nm and emission at 509 nm in black, clear-bottom 96-well plates on a Tecan Spark microplate reader with SparkControl Magellan software (Tecan Systems). The specific fluorescence was calculated for each sample by dividing the fluorescence intensity by the OD_{595}. At least two biological replicates were performed for each experiment.

Growth pattern analysis. Cultures were grown overnight in M9G1% and subsequently diluted 1:50 into new medium. Cultures were grown for 5 h and inoculated 1:40 into M9G supplemented with 6% NaCl in 96-well plates. Cultures were grown overnight with intermittent shaking in a Tecan Sunrise microplate reader and Magellan software (Tecan Systems). Ectoine was added to a final concentration of 100 μM where indicated. At least two biological replicates were performed for each experiment. Statistics were calculated using one-way analysis of variance (ANOVA) with a Tukey-Kramer *post hoc* test.

Bioinformatics analysis. Protein sequences of OpaR orthologs were downloaded from the NCBI database and aligned using the ClustalW algorithm in MEGA10. The NCBI accession numbers for each protein are BAC60779.1, AGV17442.1, AEH34083.1, OFJ17407.1, AGU95396.1, YP_205560.1, EEZ87352.1, WP_017108721.1, ADT86079.1, WP_000340102.1, EAS63745.1, EGA66814.1, and EEX95356.1. The FASTA sequences for each ectoine regulatory region were downloaded from NCBI database, and the accession numbers are listed in Table 1. Sequences were examined by the Motif Occurrence Detection Suite (MOODS) of algorithms with a given *P* value and position frequency matrix for *V. parahaemolyticus* OpaR (33). Log odds scores returned by the algorithm are the natural log of odds. The probability of binding in a given regulatory region is calculated from the odds using the following formula: probability = odds/(1 + odds).

ACKNOWLEDGMENTS

This research was supported by a National Science Foundation grant (award IOS-1656688) to E.F.B. G.J.G. was funded in part by a University of Delaware graduate fellowship award.

We thank Jessica Tague and members of the Boyd Group for constructive feedback on the manuscript.

REFERENCES

1. da Costa MS, Santos H, Galinski EA. 1998. An overview of the role and diversity of compatible solutes in *Bacteria* and *Archaea*. Adv Biochem Eng Biotechnol 61:117–153.
2. Galinski EA, Oren A. 1991. Isolation and structure determination of a novel compatible solute from the moderately halophilic purple sulfur bacterium *Ectothiorhodospira marismortui*. Eur J Biochem 198:593–598. https://doi.org/10.1111/j.1432-1033.1991.tb16055.x.
3. Galinski EA. 1995. Osmoadaptation in bacteria. Adv Microb Physiol 37:272–328.
4. Naughton LM, Blumerman SL, Carlberg M, Boyd EF. 2009. Osmoadaptation among *Vibrio* species and unique genomic features and physiological responses of *Vibrio parahaemolyticus*. Appl Environ Microbiol 75:2802–2810. https://doi.org/10.1128/AEM.01698-08.
5. Ongagna-Yhombi SY, Boyd EF. 2013. Biosynthesis of the osmoprotectant ectoine, but not glycine betaine, is critical for survival of osmotically stressed *Vibrio parahaemolyticus* cells. Appl Environ Microbiol 79:5038–5049. https://doi.org/10.1128/AEM.01008-13.
6. Ongagna-Yhombi SY, McDonald ND, Boyd EF. 2015. Deciphering the role of multiple betaine-carnitine-choline transporters in the halophile *Vibrio parahaemolyticus*. Appl Environ Microbiol 81:351–363. https://doi.org/10.1128/AEM.02402-14.
7. Louis P, Galinski EA. 1997. Characterization of genes for the biosynthesis of the compatible solute ectoine from *Marinococcus halophilus* and osmoregulated expression in *Escherichia coli*. Microbiology 143:1141–1149. https://doi.org/10.1099/00221287-143-4-1141.
8. Kuhlmann AU, Bremer E. 2002. Osmotically regulated synthesis of the compatible solute ectoine in *Bacillus pasteurii* and related *Bacillus spp*. Appl Environ Microbiol 68:772–783. https://doi.org/10.1128/aem.68.2.772-783.2002.
9. Reshetnikov AS, Khmelenina VN, Trotsenko YA. 2006. Characterization of the ectoine biosynthesis genes of haloalkalotolerant obligate methanotroph "*Methylomicrobium alcaliphilum* 20Z." Arch Microbiol 184:286–297. https://doi.org/10.1007/s00203-005-0042-z.
10. Pastor JM, Salvador M, Argandoña M, Bernal V, Reina-Bueno M, Csonka LN, Iborra JL, Vargas C, Nieto JJ, Cánovas M. 2010. Ectoines in cell stress protection: uses and biotechnological production. Biotechnol Adv 28:782–801. https://doi.org/10.1016/j.biotechadv.2010.06.005.
11. Schwibbert K, Marin-Sanguino A, Bagyan I, Heidrich G, Lentzen G, Seitz H, Rampp M, Schuster SC, Klenk HP, Pfeiffer F, Oesterhelt D, Kunte HJ. 2011. A blueprint of ectoine metabolism from the genome of the industrial producer *Halomonas elongata* DSM 2581 T. Environ Microbiol 13:1973–1994. https://doi.org/10.1111/j.1462-2920.2010.02336.x.
12. Lo C-C, Bonner CA, Xie G, D'Souza M, Jensen RA. 2009. Cohesion group approach for evolutionary analysis of aspartokinase, an enzyme that feeds a branched network of many biochemical pathways. Microbiol Mol Biol Rev 73:594–651. https://doi.org/10.1128/MMBR.00024-09.
13. Vargas C, Argandoña M, Reina-Bueno M, Rodríguez-Moya J, Fernández-Aunión C, Nieto JJ. 2008. Unraveling the adaptation responses to osmotic and temperature stress in *Chromohalobacter salexigens*, a bacterium with broad salinity tolerance. Saline Systems 4:14. https://doi.org/10.1186/1746-1448-4-14.
14. Mustakhimov II, Reshetnikov AS, Glukhov AS, Khmelenina VN, Kalyuzhnaya MG, Trotsenko YA. 2010. Identification and characterization of EctR1, a new transcriptional regulator of the ectoine biosynthesis genes in the halotolerant methanotroph *Methylomicrobium alcaliphilum* 20Z. J Bacteriol 192:410–417. https://doi.org/10.1128/JB.00553-09.
15. Shikuma NJ, Davis KR, Fong JN, Yildiz FH. 2013. The transcriptional regulator, CosR, controls compatible solute biosynthesis and transport, motility and biofilm formation in *Vibrio cholerae*. Environ Microbiol 15:1387–1399. https://doi.org/10.1111/j.1462-2920.2012.02805.x.
16. McCarter LL. 1998. OpaR, a homolog of *Vibrio harveyi* LuxR, controls opacity of *Vibrio parahaemolyticus*. J Bacteriol 180:3166–3173.
17. Henke JM, Bassler BL. 2004. Quorum sensing regulates type III secretion in *Vibrio harveyi* and *Vibrio parahaemolyticus*. J Bacteriol 186:3794–3805. https://doi.org/10.1128/JB.186.12.3794-3805.2004.
18. Gode-Potratz CJ, McCarter LL. 2011. Quorum sensing and silencing in *Vibrio parahaemolyticus*. J Bacteriol 193:4224–4237. https://doi.org/10.1128/JB.00432-11.
19. Kernell Burke A, Guthrie LT, Modise T, Cormier G, Jensen RV, McCarter LL, Stevens AM. 2015. OpaR controls a network of downstream transcription factors in *Vibrio parahaemolyticus* BB22OP. PLoS One 10:e0121863. https://doi.org/10.1371/journal.pone.0121863.
20. Zhang Y, Qiu Y, Tan Y, Guo Z, Yang R, Zhou D. 2012. Transcriptional regulation of *opaR*, *qrr*2-4, and *aphA* by the master quorum-sensing regulator OpaR in *Vibrio parahaemolyticus*. PLoS One 7:e34622. https://doi.org/10.1371/journal.pone.0034622.

Downloaded from http://aem.asm.org/ on May 1, 2020 by guest

21. Sun F, Zhang Y, Wang L, Yan X, Tan Y, Guo Z, Qiu J, Yang R, Xia P, Zhou D. 2012. Molecular characterization of direct target genes and *cis*-acting consensus recognized by quorum-sensing regulator AphA in *Vibrio parahaemolyticus*. PLoS One 7:e44210. https://doi.org/10.1371/journal.pone.0044210.
22. Kalburge SS, Carpenter MR, Rozovsky S, Boyd EF. 2017. Quorum sensing regulators are required for metabolic fitness in *Vibrio parahaemolyticus*. Infect Immun 85:e00930-16.
23. Freeman JA, Bassler BL. 1999. A genetic analysis of the function of LuxO, a two-component response regulator involved in quorum sensing in *Vibrio harveyi*. Mol Microbiol 31:665–677. https://doi.org/10.1046/j.1365-2958.1999.01208.x.
24. Freeman JA, Bassler BL. 1999. Sequence and function of LuxU: a two-component phosphorelay protein that regulates quorum sensing in *Vibrio harveyi*. J Bacteriol 181:899–906.
25. Tu KC, Bassler BL. 2007. Multiple small RNAs act additively to integrate sensory information and control quorum sensing in *Vibrio harveyi*. Genes Dev 21:221–233. https://doi.org/10.1101/gad.1502407.
26. Lilley BN, Bassler BL. 2000. Regulation of quorum sensing in *Vibrio harveyi* by LuxO and sigma-54. Mol Microbiol 36:940–954. https://doi.org/10.1046/j.1365-2958.2000.01913.x.
27. Ng WL, Bassler BL. 2009. Bacterial quorum-sensing network architectures. Annu Rev Genet 43:197–222. https://doi.org/10.1146/annurev-genet-102108-134304.
28. Rutherford ST, van Kessel JC, Shao Y, Bassler BL. 2011. AphA and LuxR/HapR reciprocally control quorum sensing in vibrios. Genes Dev 25:397–408. https://doi.org/10.1101/gad.2015011.
29. Lenz DH, Mok KC, Lilley BN, Kulkarni RV, Wingreen NS, Bassler BL. 2004. The small RNA chaperone Hfq and multiple small RNAs control quorum sensing in *Vibrio harveyi* and *Vibrio cholerae*. Cell 118:69–82. https://doi.org/10.1016/j.cell.2004.06.009.
30. van Kessel JC, Rutherford ST, Shao Y, Utria AF, Bassler BL. 2013. Individual and combined roles of the master regulators AphA and LuxR in control of the *Vibrio harveyi* quorum-sensing regulon. J Bacteriol 195:436–443. https://doi.org/10.1128/JB.01998-12.
31. Waters CM, Bassler BL. 2006. The *Vibrio harveyi* quorum-sensing system uses shared regulatory components to discriminate between multiple autoinducers. Genes Dev 20:2754–2767. https://doi.org/10.1101/gad.1466506.
32. van Kessel JC, Rutherford ST, Cong JP, Quinodoz S, Healy J, Bassler BL. 2015. Quorum sensing regulates the osmotic stress response in *Vibrio harveyi*. J Bacteriol 197:73–80. https://doi.org/10.1128/JB.02246-14.
33. Korhonen J, Martinmaki P, Pizzi C, Rastas P, Ukkonen E. 2009. MOODS: fast search for position weight matrix matches in DNA sequences. Bioinformatics 25:3181–3182. https://doi.org/10.1093/bioinformatics/btp554.
34. Oren A. 1999. Bioenergetic aspects of halophilism. Microbiol Mol Biol Rev 63:334–348.
35. Joelsson A, Kan B, Zhu J. 2007. Quorum sensing enhances the stress response in *Vibrio cholerae*. Appl Environ Microbiol 73:3742–3746. https://doi.org/10.1128/AEM.02804-06.
36. Kang Y, Goo E, Kim J, Hwang I. 2017. Critical role of quorum sensing-dependent glutamate metabolism in homeostatic osmolality and outer membrane vesiculation in *Burkholderia glumae*. Sci Rep 7:44195. https://doi.org/10.1038/srep44195.
37. Whitaker WB, Parent MA, Naughton LM, Richards GP, Blumerman SL, Boyd EF. 2010. Modulation of responses of *Vibrio parahaemolyticus* O3:K6 to pH and temperature stresses by growth at different salt concentrations. Appl Environ Microbiol 76:4720–4729. https://doi.org/10.1128/AEM.00474-10.
38. Kalburge SS, Whitaker WB, Boyd EF. 2014. High-salt preadaptation of *Vibrio parahaemolyticus* enhances survival in response to lethal environmental stresses. J Food Prot 77:246–253. https://doi.org/10.4315/0362-028X.JFP-13-241.
39. Harvell CD, Kim K, Burkholder JM, Colwell RR, Epstein PR, Grimes DJ, Hofmann EE, Lipp EK, Osterhaus AD, Overstreet RM, Porter JW, Smith GW, Vasta GR. 1999. Emerging marine diseases–climate links and anthropogenic factors. Science 285:1505–1510. https://doi.org/10.1126/science.285.5433.1505.
40. CDC. 2017. FoodNet 2015 Annual Foodborne Illness Surveillance Report. FoodNet/CDC, Atlanta, GA.
41. Turner JW, Paranjpye RN, Landis ED, Biryukov SV, Gonzalez-Escalona N, Nilsson WB, Strom MS. 2013. Population structure of clinical and environmental *Vibrio parahaemolyticus* from the Pacific Northwest coast of the United States. PLoS One 8:e55726. https://doi.org/10.1371/journal.pone.0055726.
42. Paranjpye R, Hamel OS, Stojanovski A, Liermann M. 2012. Genetic diversity of clinical and environmental *Vibrio parahaemolyticus* strains from the Pacific Northwest. Appl Environ Microbiol 78:8631–8638. https://doi.org/10.1128/AEM.01531-12.
43. Makino K, Oshima K, Kurokawa K, Yokoyama K, Uda T, Tagomori K, Iijima Y, Najima M, Nakano M, Yamashita A, Kubota Y, Kimura S, Yasunaga T, Honda T, Shinagawa H, Hattori M, Iida T. 2003. Genome sequence of *Vibrio parahaemolyticus*: a pathogenic mechanism distinct from that of *V. cholerae*. Lancet 361:743–749. https://doi.org/10.1016/S0140-6736(03)12659-1.
44. Gibson DG. 2011. Enzymatic assembly of overlapping DNA fragments. Methods Enzymol 498:349–361. https://doi.org/10.1016/B978-0-12-385120-8.00015-2.
45. Horton RM, Hunt HD, Ho SN, Pullen JK, Pease LR. 1989. Engineering hybrid genes without the use of restriction enzymes: gene splicing by overlap extension. Gene 77:61–68. https://doi.org/10.1016/0378-1119(89)90359-4.
46. Livak KJ, Schmittgen TD. 2001. Analysis of relative gene expression data using real-time quantitative PCR and the $2^{-\Delta\Delta CT}$ method. Methods 25:402–408. https://doi.org/10.1006/meth.2001.1262.
47. Karunakaran R, Mauchline TH, Hosie AH, Poole PS. 2005. A family of promoter probe vectors incorporating autofluorescent and chromogenic reporter proteins for studying gene expression in Gram-negative bacteria. Microbiology 151:3249–3256. https://doi.org/10.1099/mic.0.28311-0.
48. Haardt M, Kempf B, Faatz E, Bremer E. 1995. The osmoprotectant proline betaine is a major substrate for the binding-protein-dependent transport system ProU of *Escherichia coli* K-12. Mol Gen Genet 246:783–786. https://doi.org/10.1007/bf00290728.
49. Dehio C, Meyer M. 1997. Maintenance of broad-host-range incompatibility group P and group Q plasmids and transposition of Tn*5* in *Bartonella henselae* following conjugal plasmid transfer from *Escherichia coli*. J Bacteriol 179:538–540. https://doi.org/10.1128/jb.179.2.538-540.1997.
50. Philippe N, Alcaraz JP, Coursange E, Geiselmann J, Schneider D. 2004. Improvement of pCVD442, a suicide plasmid for gene allele exchange in bacteria. Plasmid 51:246–255. https://doi.org/10.1016/j.plasmid.2004.02.003.
51. Kovach ME, Phillips RW, Elzer PH, Roop RM, II, Peterson KM. 1994. pBBR1MCS: a broad-host-range cloning vector. Biotechniques 16:800–802.
52. Liu J, Li F, Rozovsky S. 2013. The intrinsically disordered membrane protein selenoprotein S is a reductase *in vitro*. Biochemistry 52:3051–3061. https://doi.org/10.1021/bi4001358.

Downloaded from http://aem.asm.org/ on May 1, 2020 by guest